Eur. Phys. J. C 6, 671–680 (1999)
DOI 10.1007/s100529800945

THE EUROPEAN PHYSICAL JOURNAL C

Single particle spectra in deep inelastic scattering as a probe of small x dynamics

J. Kwiecinski[a], S.C. Lang[b], A.D. Martin

Department of Physics, University of Durham, Durham, DH1 3LE, UK

Received: 4 May 1998 / Published online: 21 August 1998

Abstract. We study the transverse momentum (p_T) spectrum of charged particles produced in deep inelastic scattering (DIS) at small Bjorken x in the central region between the current jet and the proton remnants. We calculate the spectrum at large p_T with the BFKL $\ln(1/x)$ resummation included and then repeat the calculation with it omitted. We find that data favour the former. We normalize our BFKL predictions by comparing with HERA data for DIS containing a forward jet. The shape of the x distribution of DIS + jet data is also well described by BFKL dynamics.

1 Introduction

An intriguing feature of the measurements at HERA in the small x domain is the possible existence of significant $\ln(1/x)$ effects. A major part of the rise observed for the structure function F_2 with decreasing x may be attributed to the resummation of the leading $\ln(1/x)$ 'BFKL' [1] contributions. An excellent unified BFKL/GLAP fit of F_2 in the HERA regime has recently been obtained using a "flat in x" input [2], and the rise due to BFKL-type effects has been quantified within this description. However, the growth of F_2 with decreasing x can be described equally well by pure GLAP [3] $\ln(Q^2)$ evolution from suitably chosen input parton distributions so the main origin of the rise is still an open question. The observable F_2 is too inclusive to distinguish between these alternatives. The study of deep inelastic scattering (DIS) events containing an isolated forward jet [4,5] is a better discriminator of the underlying small x dynamics. The process is sketched in Fig. 1a. In this case we effectively study DIS off known parton distributions and so we avoid the ambiguity in the choice of the input distributions. The method is theoretically attractive. The summation of the leading $\ln(1/x)$ contributions gives an $(x/x_j)^{-\lambda}$ behaviour of the BFKL ladder connecting the photon to parton a. Here x is Bjorken x and x_j is the fraction of the proton's longitudinal momentum carried by the parton jet. An unambiguous measurement of the exponent λ looks feasible. In practice a major problem is the identification of the jet due to parton a, and the measurement of its momentum, when it is close to the remnants of the proton. Typically the clean observation of the jet requires $x_j \lesssim 0.1$ and so in this process we lose about a factor of 10 in the 'small x reach' of HERA.

Besides the $x^{-\lambda}$ growth as x decreases along the BFKL ladder, a second characteristic feature is the diffusion in $\ln k_T^2$ where k_T are the transverse momenta of the gluons emitted along the chain. One way the diffusion manifests itself is in an enhancement of the transverse energy (E_T) flow in the central region between the current jet and the proton remnants [6], see Fig. 1b. In principle the diffusion can enhance E_T from both the 'upper' and 'lower' BFKL gluon ladders, which are denoted by Φ and f in Fig. 1b. However, the x reach at HERA is insufficient to fully develop the $\ln k_T^2$ diffusion in both ladders simultaneously. Nevertheless, the effect is quite appreciable giving at the *parton* level an energy flow $E_T \lesssim 2$ GeV/unit of rapidity. However the clean parton level prediction can in practice be masked or mimicked by the effects of hadronization. Thus, although the prediction for E_T is in agreement with observations [7] we cannot definitely conclude that it is due to $\ln(1/x)$ resummations.

An interesting way to overcome this ambiguity is to consider the emission of single particles at relatively large transverse momentum p_T in the central region [8]. The single particle spectrum at sufficiently large values of p_T should be much more immune from hadronization and more directly reflect the $\ln k_T^2$ diffusion from the BFKL ladders.

The outline of the contents of the paper is as follows. In Sect. 2 we use the data for the process DIS + forward jet to normalise the BFKL function Φ shown in Fig. 1a. To be precise we numerically solve the BFKL equation for Φ using the amplitude $\Phi^{(0)}$ for the quark box (and crossed box) as input at a value z_0 of $z = x/x_j$ which is chosen so that the resulting Φ reproduces the DIS + jet data. Also, for completeness, we present in Sect. 2, an ana-

[a] On leave from H. Niewodniczanski Institute of Nuclear Physics, Department of Theoretical Physics, ul. Radzikowskiego 152, 31-342 Krakow, Poland

[b] *Present address:* Institute for Theoretical Physics, Universität Regensburg, 93053 Regensburg, Germany

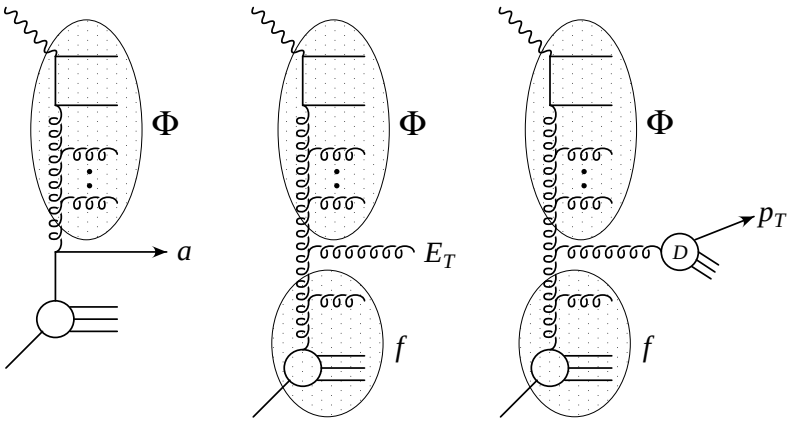

(a) DIS + jet (b) E_T flow (c) Single particle spectrum

Fig. 1. Diagrammatic representation of **a** the deep inelastic + forward jet, **b** the E_T flow, and **c** the single particle spectrum measurement

lytic form for Φ which is valid for fixed α_S, and which has been the basis for a recent analysis. In Sect. 3 we give the formula necessary to calculate the transverse momentum (p_T) spectrum of single particles produced in the central region. The process is shown in Fig. 1c. The predictions for the p_T spectra (with and without the BFKL effects included) are compared with HERA data. Finally in Sect. 4 we give our conclusions.

2 DIS + forward jet events

We first calculate the cross section for DIS containing a forward identified jet. This so-called "Mueller" process is a valuable probe of small x dynamics in its own right. We compare with HERA data to normalise the function Φ shown in Fig. 1a. There are uncertainties in the normalisation, and even the shape of the x distribution is dependent on subleading $\ln(1/x)$ corrections.

The variables of the process are shown in Fig. 2. As usual the variables x and y are given by $x = Q^2/2p\cdot q$ and $y = p\cdot q/p_e\cdot p$ where p, p_e and q denote the four momenta of the proton, the incident electron and the virtual photon respectively, and $Q^2 \equiv -q^2$. The variables x_j and k_{jT} are the longitudinal momentum fraction and transverse momentum carried by the forward jet. The differential cross section is given by [4]

$$\frac{\partial\sigma_j}{\partial x\partial Q^2} = \int dx_j \int dk_{jT}^2 \frac{4\pi\alpha^2}{xQ^4} \times \left[(1-y)\,\frac{\partial F_2}{\partial x_j \partial k_{jT}^2} + \frac{1}{2}y^2 \frac{\partial F_T}{\partial x_j \partial k_{jT}^2}\right] \quad (1)$$

where the differential structure functions have the following form

$$\frac{\partial^2 F_i}{\partial x_j \partial k_{jT}^2} = \frac{3\alpha_S(k_{jT}^2)}{\pi k_{jT}^2} \sum_a f_a\left(x_j, k_{jT}^2\right) \times \Phi_i\left(\frac{x}{x_j}, k_{jT}^2, Q^2\right) \quad (2)$$

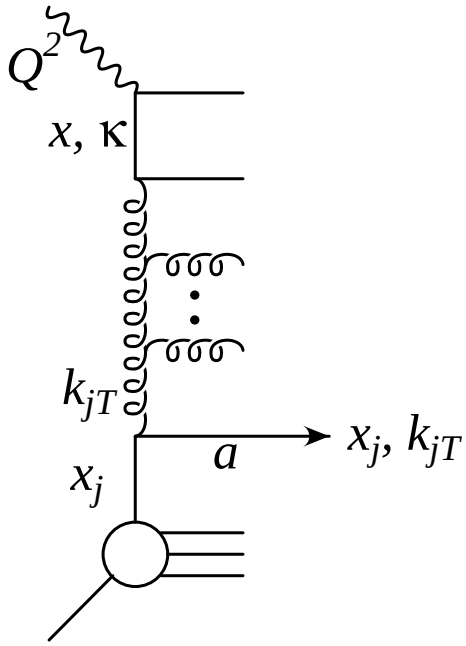

Fig. 2. Diagrammatic representation of a deep inelastic + forward jet event

for $i = T, L$ and $F_2 = F_T + F_L$. We have assumed strong ordering at the parton a - gluon vertex. Assuming also t-channel pole dominance the sum over the parton distributions is given by

$$\sum_a f_a = g + \frac{4}{9}\sum_q (q + \bar{q})\,. \quad (3)$$

Recall that these parton distributions are to be evaluated at (x_j, k_{jT}^2) and that x_j is taken as large as is experimentally feasible. The data that we describe below have $x_j > 0.035$. For these values of x_j the partons are reliably determined from the global analyses, so there are no ambiguities arising from a non-perturbative input.

The functions $\Phi_i(x/x_j, k_{jT}^2, Q^2)$ describe the virtual γ + virtual gluon fusion process including the ladder formed

from the gluon chain of Fig. 2. They can be obtained by solving the BFKL equations

$$\Phi_i(z,k_T^2,Q^2)=\Phi_i^{(0)}(z,k_T^2,Q^2)+\overline{\alpha}_S\int_z^1\frac{dz'}{z'}\int\frac{d^2q}{\pi q^2}\times\left[\Phi_i(z',(\boldsymbol{q}+\boldsymbol{k_T})^2,Q^2))-\Phi_i(z',k_T^2,Q^2)\Theta(k_T^2-q^2)\right] \quad (4)$$

where $\overline{\alpha}_S\equiv 3\alpha_S/\pi$. The inhomogeneous or driving terms $\Phi_i^{(0)}$ correspond to the sum of the quark box and crossed-box contributions. For small z we have

$$\Phi_i^{(0)}(z,k_T^2,Q^2)\approx\Phi_i^{(0)}(z=0,k_T^2,Q^2)\equiv\Phi_i^{(0)}(k_T^2,Q^2). \quad (5)$$

We evaluate the $\Phi_i^{(0)}$ by expanding the four momentum in terms of the basic light-like four momenta p and $q'\equiv q+xp$. For example, the quark momentum κ in the box (see Fig. 2) has the Sudakov decomposition

$$\kappa=\alpha p-\beta q'+\boldsymbol{\kappa}_T\ .$$

We carry out the integration over the box diagrams, subject to the quark mass-shell constraints, and find

$$\begin{aligned}\Phi_T^{(0)}(k_T^2,Q^2)&=2\sum_q e_q^2\frac{\alpha_S}{4\pi^2}\frac{Q^2}{k_T^2}\int_0^1 d\beta\int d^2\kappa_T\\&\times\left\{\left[\beta^2+(1-\beta)^2\right]\left(\frac{\kappa_T^2}{D_1^2}-\frac{\boldsymbol{\kappa}_T.(\boldsymbol{\kappa}_T-\boldsymbol{k}_T)}{D_1D_2}\right)\right.\\&\left.+m_q^2\left(\frac{1}{D_1^2}-\frac{1}{D_1D_2}\right)\right\}\\\Phi_L^{(0)}(k_T^2,Q^2)&=2\sum_q e_q^2\frac{\alpha_S}{\pi^2}\frac{Q^4}{k_T^2}\int_0^1 d\beta\int d^2\kappa_T\beta^2(1-\beta)^2\\&\times\left(\frac{1}{D_1^2}-\frac{1}{D_1D_2}\right)\ .\end{aligned} \quad (6)$$

where the denominators D_i are of the form

$$\begin{aligned}D_1&=\kappa_T^2+\beta(1-\beta)Q^2+m_q^2\\D_2&=(\boldsymbol{\kappa}_T-\boldsymbol{k}_T)^2+\beta(1-\beta)Q^2+m_q^2\ .\end{aligned} \quad (7)$$

The light u, d and s quarks are taken to be massless ($m_q=0$) and the charm quark to have mass $m_c=1.4$ GeV.

2.1 Analytic form of Φ for fixed α_S

We solve the BFKL equation for Φ numerically, which allows the use of running α_S and the inclusion of a charm quark mass. However, it is informative to recall the analytic solution which can be obtained if α_S is fixed and we assume that the quarks are massless. The first step is to rewrite the driving terms (6) for $m_q=0$ in the form

$$\Phi_T^{(0)}(k_T^2,Q^2)=\sum_q e_q^2\frac{\alpha_S}{4\pi}Q^2\int_0^1 d\lambda\int_0^1 d\beta\times\frac{[\beta^2+(1-\beta)^2][\lambda^2+(1-\lambda)^2]}{[\lambda(1-\lambda)k_T^2+\beta(1-\beta)Q^2]} \quad (8)$$

$$\Phi_L^{(0)}(k_T^2,Q^2)=\sum_q e_q^2\frac{2\alpha_S}{\pi}Q^2\int_0^1 d\lambda\int_0^1 d\beta\times\frac{\lambda(1-\lambda)\beta(1-\beta)}{[\lambda(1-\lambda)k_T^2+\beta(1-\beta)Q^2]} \quad (9)$$

where λ is the Feynman parameter which appears in the representation

$$\frac{1}{D_1D_2}=\int_0^1 d\lambda\frac{1}{[\lambda D_1+(1-\lambda)D_2]^2}. \quad (10)$$

We see that, for fixed α_S and $m_q=0$, the $\Phi_i^{(0)}$ are functions of a single dimensionless variable $r=Q^2/k_T^2$. We may therefore represent the driving terms $\Phi_i^{(0)}(Q^2/k_T^2)$ in terms of their Mellin transforms $\tilde{\Phi}_i^{(0)}(\gamma)$

$$\Phi_i^{(0)}(r)=\frac{1}{2\pi i}\int_{\frac{1}{2}-i\infty}^{\frac{1}{2}+i\infty}d\gamma\tilde{\Phi}_i^{(0)}(\gamma)r^\gamma \quad (11)$$

where $i=L,T$ and $r\equiv Q^2/k_T^2$. The Mellin transform is useful since it diagonalizes the BFKL equation (4). The solutions for fixed coupling α_S may therefore be written

$$\Phi_i(z,k_T^2,Q^2)=\frac{1}{2\pi i}\int_{\frac{1}{2}-i\infty}^{\frac{1}{2}+i\infty}d\gamma\left(\frac{Q^2}{k_T^2}\right)^\gamma\times\exp(\overline{\alpha}_SK(\gamma)\ln\frac{1}{z})\tilde{\Phi}_i^{(0)}(\gamma) \quad (12)$$

where $\overline{\alpha}_S\equiv 3\alpha_S/\pi$ and $K(\gamma)$ is the Mellin transform of the kernel of the BFKL equation

$$K(\gamma)=2\Psi(1)-\Psi(\gamma)-\Psi(1-\gamma) \quad (13)$$

with $\Psi(\gamma)\equiv\Gamma'(\gamma)/\Gamma(\gamma)$. The functions $\tilde{\Phi}_i^{(0)}(\gamma)$ are obtained by inserting (8) and (9) into the inverse relation to (11). We find

$$\begin{aligned}\tilde{\Phi}_T^{(0)}(\gamma)&=\sum_q e_q^2\frac{\alpha_S}{4\pi}\int_0^\infty drr^{-\gamma}\int_0^1 d\lambda\int_0^1 d\beta\\&\times\frac{[\beta^2+(1-\beta)^2][\lambda^2+(1-\lambda)^2]}{[\lambda(1-\lambda)+\beta(1-\beta)r]}\\&=\sum_q e_q^2\frac{\alpha_S}{\sin\pi\gamma}B(\gamma+2,\gamma)B(3-\gamma,1-\gamma)\end{aligned} \quad (14)$$

$$\begin{aligned}\tilde{\Phi}_L^{(0)}(\gamma)&=\sum_q e_q^2\frac{2\alpha_S}{\pi}\int_0^\infty drr^{-\gamma}\int_0^1 d\lambda\int_0^1 d\beta\\&\times\frac{\lambda(1-\lambda)\beta(1-\beta)}{[\lambda(1-\lambda)+\beta(1-\beta)r]}\\&=\sum_q e_q^2\frac{2\alpha_S}{\sin\pi\gamma}B(-\gamma+2,-\gamma+2)B(\gamma+1,\gamma+1)\end{aligned} \quad (15)$$

where $B(x,y) \equiv \Gamma(x)\Gamma(y)/\Gamma(x+y)$. The derivation of the analytic formula relies on α_S being fixed. This approach has been used by Bartels et al. [9] to estimate the DIS + forward jet cross section taking the coupling $\alpha_S(k_T^2)$ in formulae (12). The prediction has the general shape of the H1 data as a function of x, but the calculated cross section exceeds the data by some 20% [10].

In the $z \to 0$ limit the formulae reduce to the conventional $z^{-\lambda}$ BFKL behaviour

$$\Phi_i(z,k_T^2,Q^2) \sim z^{-\overline{\alpha}_S K(\frac{1}{2})} \left(\frac{Q^2}{k_T^2}\right)^{\frac{1}{2}} \times \frac{\tilde{\Phi}_i^{(0)}(\gamma=\frac{1}{2})}{(\overline{\alpha}_S K''(\frac{1}{2}) \ln 1/z)^{\frac{1}{2}}} \tag{16}$$

where for simplicity we have omitted the Gaussian diffusion factor in $\ln(k_T^2/Q^2)$. If we evaluate the various functions at $\gamma = \frac{1}{2}$ we obtain

$$\Phi_T(z,k_T^2,Q^2) = \frac{9\pi^2}{512} \frac{2\sum e_q^2 \alpha_S^{\frac{1}{2}}}{\sqrt{21\zeta(3)/2}} \left(\frac{Q^2}{k_T^2}\right)^{\frac{1}{2}} \times \frac{z^{-\lambda}}{\sqrt{\ln(1/z)}} \left[1 + O\left(\frac{1}{\ln(1/z)}\right)\right]$$
$$\Phi_L(z,k_T^2,Q^2) = \frac{2}{9}\Phi_T(z,k_T^2,Q^2) \tag{17}$$

where $\lambda = \overline{\alpha}_S K(\frac{1}{2}) = \overline{\alpha}_S 4 \ln 2$.

2.2 Normalisation of Φ and the description of DIS + jet data

Our calculation of the DIS + forward jet process differs from that of [9] in that we numerically solve the BFKL equations. Therefore, we are able to explicitly include the $m_c \neq 0$ charm contribution. We also allow the coupling α_S to run. To be precise we solve the BFKL equation (4) rewritten in terms of the modified function $\overline{\alpha}_S(k_T^2)\Phi_i(z,k_T^2,Q^2)$ following the prescription that was used in [5]. This choice of scale for α_S is consistent with the double logarithm limit and with the NLO $\ln(1/x)$ analysis of [11]. Formally by allowing the coupling to run we introduce effects which go beyond the LO $\ln(1/x)$ approximation. However they constitute only part of the NLO $\ln(1/x)$ contribution and the remaining next-to-leading terms may still affect the solution of the (modified) BFKL equation.

We determine the functions Φ_i for $z < z_0$ by solving the BFKL equation as described in [5] starting from the boundary condition

$$\Phi_i(z_0,k_T^2,Q^2) = \Phi_i^{(0)}(z_0,k_T^2,Q^2) \approx \Phi_i^{(0)}(k_T^2,Q^2) \tag{18}$$

where $\Phi_i^{(0)}(k_T^2,Q^2)$ are the contributions of the quark box (and crossed box) given in (6). We take u,d,s to be massless and the charm quark to have mass $m_c = 1.4$GeV in the summation over the quarks. We then use (1) integrated over x and Q^2 and (2) to calculate the DIS + forward jet rate corresponding to the cuts used in the H1 measurement. That is the forward jet is constrained to the region

$$7^\circ < \theta_j < 20^\circ, \quad E_j > 28.7\text{GeV}, \quad k_{jT} > 3.5\text{GeV},$$

whereas the outgoing electron must lie in the domain

$$160^\circ < \theta_e' < 173^\circ, \quad E_e' > 11\text{GeV}, \quad y > 0.1$$

in the HERA frame. Finally H1 require $\frac{1}{2}Q^2 < k_{jT}^2 < 2Q^2$. The BFKL calculation is compared with the data [10] in bins of size $\Delta x = 5 \times 10^{-4}$ in Fig. 3. We take the cut-off on the dq^2 integration in (4) to be $q^2 > k_0^2 = 1\text{GeV}^2$. The parameter z_0 is then adjusted to give a satisfactory normalization of the calculation. We find that the H1 data require $z_0 \simeq 0.15$. The predicted shape of the distribution is in good agreement with the data. The sensitivity of the calculated cross section to different choices of k_0^2 and z_0 is shown for two different x bins in Fig. 4. We see that the calculated values are relatively insensitive to the choice of k_0^2 and that $z_0 = 0.15$ is preferred to $z_0 = 0.1$.

We note that the DIS + forward jet measurement is, in principle, a very clear test of possible BFKL resummation effects and that recent data from the H1 collaboration at HERA confirm the importance of such $\ln(1/x)$ effects. Theoretical analyses of this process [9,12] have shown that the data cannot be described by fixed-order QCD which underestimates the experimental results and gives a cross-section which rises significantly less steeply with decreasing x than the measured values. The BFKL resummation effects are clearly needed.

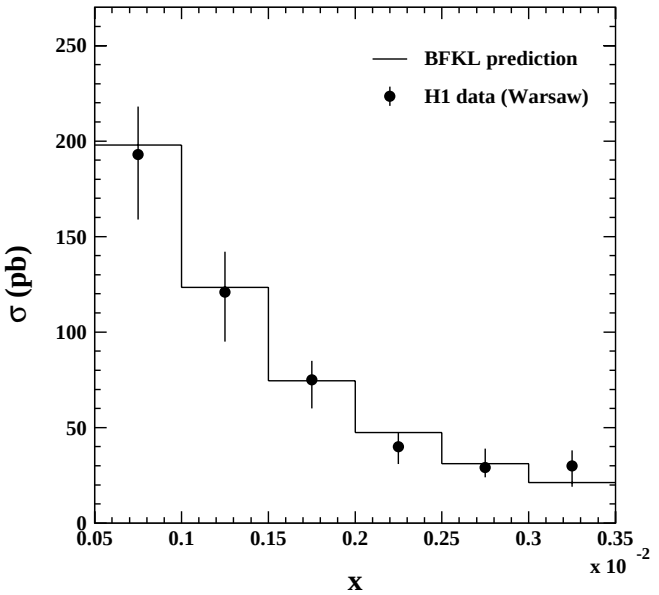

Fig. 3. The deep inelastic + forward jet cross section in pb integrated over bins of size 5×10^{-4} in x compared to the H1 data presented at the Warsaw conference [10]. As in the H1 measurement the forward jet was required to fulfil $7^\circ < \theta_j < 20^\circ$, $E_j > 28.7$ GeV, and $k_{jT} > 3.5$ GeV. The electron acceptance region is limited by $160^\circ < \theta_e' < 173^\circ$, $E_e' > 11$ GeV, and $y > 0.1$ in the HERA frame

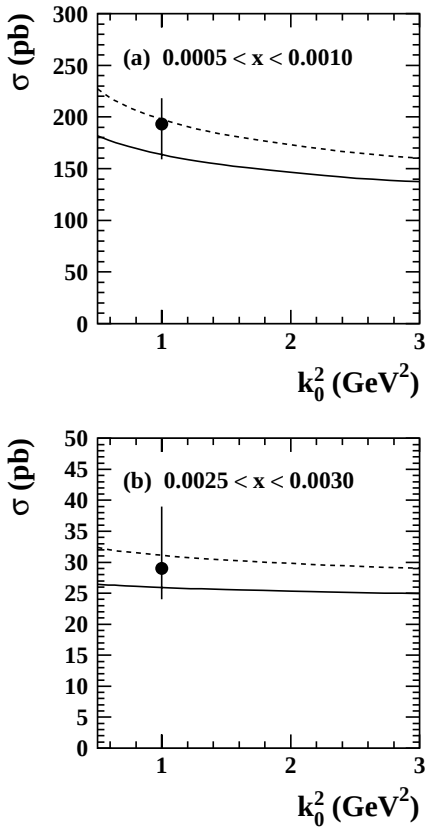

Fig. 4. The dependence of the DIS + jet cross section calculated from the BFKL equation (4) to the cut-off k_0^2 on the dq^2 integration and to the starting value z_0 at which the boundary conditions are specified. The dashed and continuous curves correspond to $z_0 = 0.15$ and 0.1 respectively. MRS(R2) partons [15] are used. The H1 measurements [13] in the two x bins are plotted at $k_0^2 = 1\text{GeV}^2$

3 Single particle p_T spectra

We first use Fig. 1c to obtain the differential cross section for the production of a hadron of transverse momentum p_T and longitudinal momentum fraction x_h. Then we calculate the charged particle spectra relevant to the recent observations at HERA [13].

3.1 The cross section for charged particle production

The cross-section for single particle production is obtained by convoluting the inclusive cross-section for the production of a single parton with the parton fragmentation function. The differential cross section for the inclusive production of a single parton of longitudinal momentum fraction x_j and transverse momentum k_{jT} has the generic form of (1). We have

$$\frac{\partial\sigma_j}{\partial x_j \partial k_{jT}^2 \partial x \partial Q^2} = \frac{4\pi\alpha^2}{xQ^4}\left[(1-y)\frac{\partial F_2}{\partial x_j \partial k_{jT}^2} + \frac{1}{2}y^2 \frac{\partial F_T}{\partial x_j \partial k_{jT}^2}\right] . \quad (19)$$

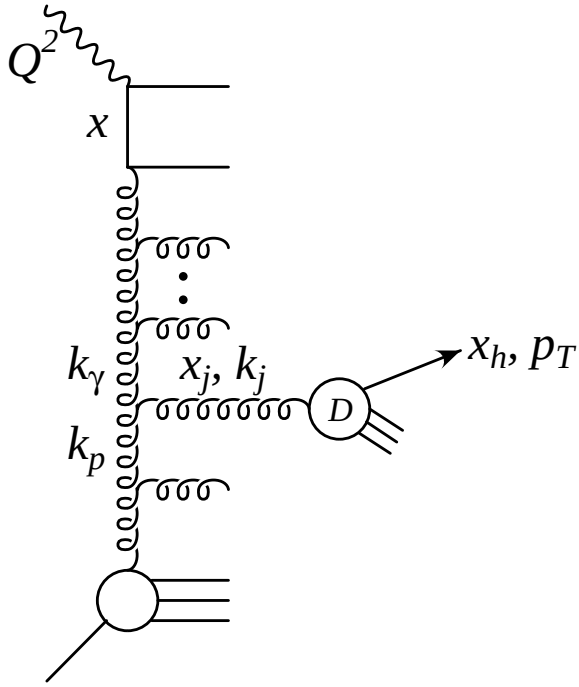

Fig. 5. Diagrammatic representation of the cross section for emission of a high transverse momentum p_T particle

Now for small x, and in the central region away from the current jet and the proton remnants, we expect gluonic partons to dominate where the gluons are radiated within the BFKL ladder. The differential structure functions occurring in (19) are then given by

$$x_j \frac{\partial F_i}{\partial x_j \partial k_j^2} = \int \frac{d^2k_p}{\pi k_p^4} \int \frac{d^2k_\gamma}{k_\gamma^2}\left[\frac{\overline{\alpha}_S(k_j^2)k_p^2 k_\gamma^2}{k_j^2}\right] \times f(x_j, k_p^2)\Phi_i\left(\frac{x}{x_j}, k_\gamma^2, Q^2\right)\delta^2(k_j - k_p - k_\gamma) \quad (20)$$

with $i = T, L$ and where for simplicity we have omitted the subscript T from the gluon transverse momenta, k_{jT}, k_{pT} and $k_{\gamma T}$, see Fig. 5. The functions Φ_i are those of Sect. 2 which control the DIS + forward jet rate, while f is the unintegrated gluon distribution which satisfies the BFKL equation

$$-z\frac{\partial f(z,k^2)}{\partial z} = \overline{\alpha}_S \int \frac{d^2q}{\pi q^2}\left[\frac{k^2}{(\boldsymbol{q}+\boldsymbol{k})^2} f(z,(\boldsymbol{q}+\boldsymbol{k})^2) - f(z,k^2)\Theta(k^2-q^2)\right] . \quad (21)$$

The expression in square brackets in (20) arises from the (square of the) BFKL vertex for real gluon emission, see Fig. 5.

In practice we evolve (21) down in z from the boundary condition

$$f(\overline{z}_0, k^2) = f^{AP}(\overline{z}_0, k^2) = \frac{\partial\left[\overline{z}_0 g^{AP}(\overline{z}_0, k^2)\right]}{\partial \ln(k^2/k_0^2)} \quad (22)$$

where here $z = \overline{z}_0$ with[1] $\overline{z}_0 = 10^{-2}$, and where g^{AP} is the conventional gluon distribution obtained from a global set of partons. As before we allow the coupling to run, that is we take $\alpha_S(k^2)$ in (21). Moreover, we impose an infrared cut-off $k_0^2 = 1\text{GeV}^2$. That is we require the arguments of f to satisfy $k^2 > k_0^2$ and $(\boldsymbol{k}+\boldsymbol{q})^2 > k_0^2$. Similarly, the integrations in (20) are restricted to the regions $k_p^2, k_\gamma^2 > k_0^2$. We may include the contribution ΔF_i from the region $k_p^2 < k_0^2$ by assuming the strong ordering approximation, $k_p^2 \ll k_\gamma^2 \sim k_j^2$, at the gluon vertex. This contribution to (20) then becomes

$$x_j \frac{\partial(\Delta F_i)}{\partial x_j \partial k_j^2} = \overline{\alpha}_S(k_j^2) \int^{k_0^2} \frac{dk_p^2}{k_p^2} f(x_j, k_p^2) \Phi_i\left(\frac{x}{x_j}, k_j^2, Q^2\right) = \overline{\alpha}_S(k_j^2) \frac{x_j g(x_j, k_0^2)}{k_j^2} \Phi_i\left(\frac{x}{x_j}, k_j^2, Q^2\right). \quad (23)$$

Most of the time, however, for the calculation relevant to the HERA data, the variable x_j is not small enough for the BFKL equation to be applicable for the function f. In these cases, that is when $x_j > \overline{z}_0$, we therefore again assume strong ordering $k_p^2 \ll k_\gamma^2 \sim k_j^2$. In addition we include the contributions from quark and antiquark jets. We then obtain

$$x_j \frac{\partial F_2}{\partial x_j \partial k_j^2} = \overline{\alpha}_S(k_j^2) \frac{x_j\left[g + \frac{4}{9}\sum_q (q+\bar{q})\right]}{k_j^2} \times \Phi_i\left(\frac{x}{x_j}, k_j^2, Q^2\right), \quad (24)$$

where the parton distributions are to be evaluated[2] at (x_j, k_j^2). The differential cross section for single particle (h) production is obtained by convoluting the jet cross section with the fragmentation functions D for the parton $\to h$ transition

$$\frac{\partial \sigma_h}{\partial x_h \partial p_T^2 \partial x \partial Q^2} = \int_{x_h}^1 dz \int dx_j \int dk_j^2 \delta(x_h - z x_j) \times \delta(p_T - z k_j) \left\{ \frac{\partial \sigma_g}{\partial x_j \partial k_j^2 \partial x \partial Q^2} D_g^h(z, \mu^2) + \frac{4}{9} \sum_q \left[\frac{\partial \sigma_q}{\partial x_j \partial k_j^2 \partial x \partial Q^2} D_q^h(z, \mu^2) + \frac{\partial \sigma_{\overline{q}}}{\partial x_j \partial k_j^2 \partial x \partial Q^2} D_{\overline{q}}^h(z, \mu^2) \right] \right\} \quad (25)$$

where σ_g, σ_q and $\sigma_{\overline{q}}$ are the contributions to the cross section σ_j for gluon, quark and antiquark jets respectively. The fragmentation scale μ^2 is of the order of k_j^2. The cross section for charged particle production is obtained by summing over all possible charged hadrons h.

3.2 Predictions for the single particle p_T spectra

The data for the single (charged) particle p_T spectra are presented in the form $(dn/dp_T)/N$ where n is the multiplicity and N the total number of charged particles in a given x, Q^2 bin [13]. To calculate this p_T spectrum we evaluate

$$\frac{1}{N}\frac{dn}{dp_T} = \left(\sum_h \frac{\partial \sigma_h}{\partial p_T \partial x \partial Q^2}\right) \Big/ \frac{\partial \sigma_{tot}}{\partial x \partial Q^2}. \quad (26)$$

where $\partial \sigma_h / \partial p_T \partial x \partial Q^2$ is obtained from (25) by integrating over x_h. We take the central values of x, Q^2 in the bin. The integration limits are fixed by the limits on the pseudorapidity interval under consideration. To be precise we use

$$x_h = \sqrt{\frac{x}{Q^2}} p_T e^{-\eta} \quad (27)$$

where η is the pseudorapidity of the charged particle, $\eta = -\ln\tan(\theta/2)$ with θ the angle with respect to the virtual photon direction. Finally we calculate the total differential cross section $\partial \sigma_{tot}/\partial x \partial Q^2$ in (26) from the structure functions F_2 and F_L given by the MRS(R2) [15] set of parton distributions.

Our aim is to make an absolute BFKL-based prediction to compare with the p_T spectra observed by the H1 collaboration. There is, however, an inherent uncertainty in the normalisation due to the imposition of an infrared cut-off on the BFKL transverse momentum integrations (or due to other possible treatments of the non-perturbative region). To overcome this problem we follow the procedure described in Sect. 2.2 and fix the parameters occurring in the calculation of the BFKL functions Φ_i by requiring the prediction for the DIS + jet cross section to give the correct normalization of the H1 forward jet measurements. The next step is to use the functions Φ_i obtained in this way in the computation of the differential structure functions from (20), (23) and (24). In this way we are able to calculate a normalized p_T spectrum from (26).

The BFKL prediction for the single particle spectra may be compared with the result which would be obtained if the BFKL gluon radiation is neglected. That is in (20), (23) and (24) we replace the functions Φ_i which describe the solution of the BFKL equation with the boundary condition given by the quark box $\Phi_i^{(0)}$ only. In addition we now also assume strong ordering for $x_j < \overline{z}_0$ and carry out the k_p^2 integration in (20). This amounts to assuming that in a fixed-order treatment the dominant subprocess is $\gamma g \to q\overline{q}g$. In our calculation the κ integration is infrared finite since we allow for the virtuality of the incoming and exchanged gluons.

So we are now in the position to give a BFKL prediction for the single particle spectra which can be compared

[1] The choice of $\overline{z}_0 = 0.01$ marks the boundary below which BFKL effects may not be neglected. It was used in the early small x analyses [6,14] and is supported by a recent unified BFKL/DGLAP study [2] of F_2 data

[2] For these values of $x_j, x_j > 0.01$, the partons are reliably determined from the global analyses of deep inelastic and related hard scattering data

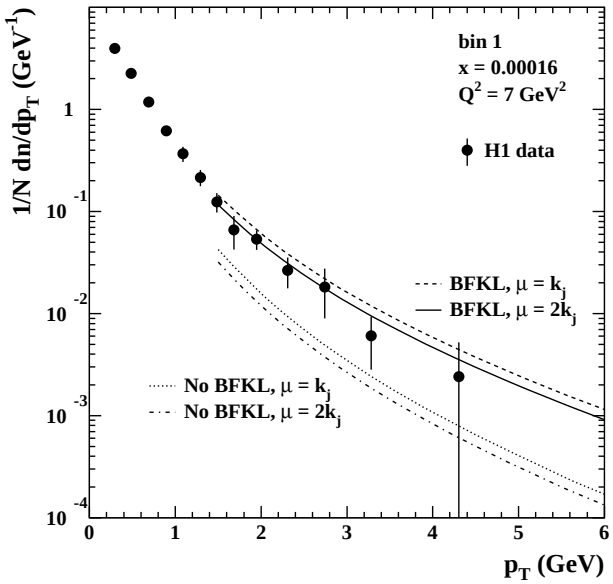

Fig. 6. The transverse momentum spectrum of charged particles (π^+, π^-, K^+, K^-) in the pseudorapidity interval $0.5 < \eta < 1.5$ in the virtual photon-proton centre-of-mass frame. The results are shown for kinematic bin 1 with the central values $x = 1.6 \times 10^{-4}$ and $Q^2 = 7$ GeV^2. The continuous and the dashed curves show the spectra obtained with Φ_i and f calculated from the BFKL equation. They only differ in the choice of fragmentation scale: for the continuous curve the fragmentation functions were evaluated at scale $\mu^2 = (2k_j)^2$ and for the dashed curve at scale $\mu^2 = k_j^2$. When BFKL radiation is neglected in the calculation of the p_T spectra, i.e. when the quark box approximation $\Phi_i = \Phi_i^{(0)}$ is used and strong ordering at the gluon vertex is assumed, then the dash-dotted and dotted curves are obtained. The fragmentation functions were evaluated at scales $2k_j$ and k_j respectively. The data points shown are from the H1 measurement of the charged particle spectra [13]

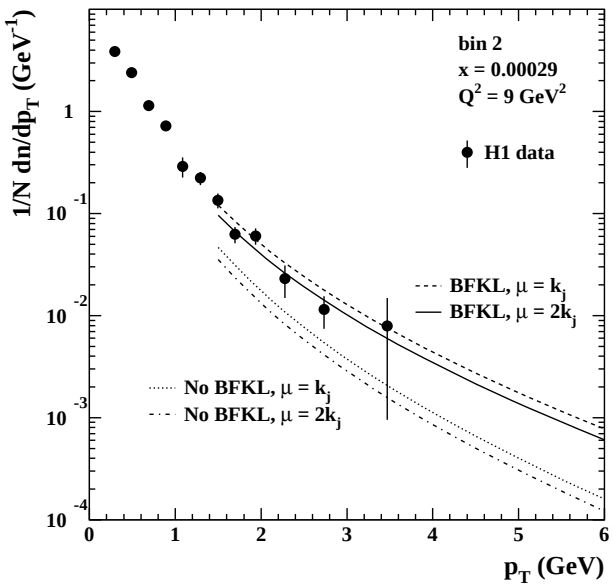

Fig. 7. As Fig. 5, but for kinematic bin 2, $x = 2.9 \times 10^{-4}$ and $Q^2 = 9$ GeV^2

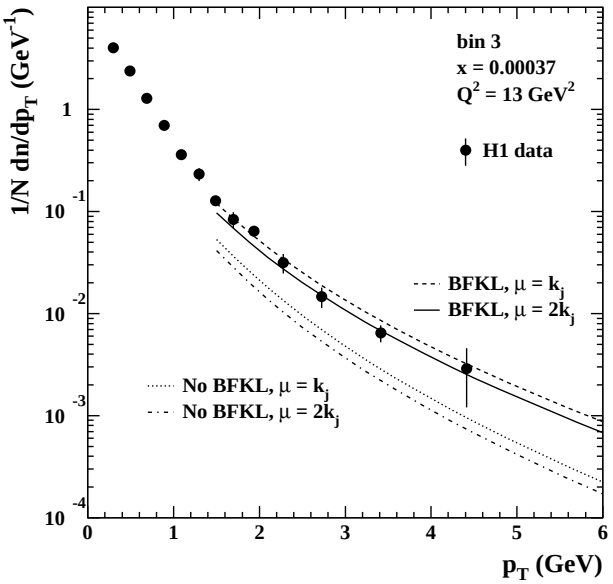

Fig. 8. As Fig. 5, but for kinematic bin 3, $x = 3.7 \times 10^{-4}$ and $Q^2 = 13$ GeV^2

with the H1 data. In their measurement the H1 collaboration collected data in nine different kinematic bins in two pseudorapidity intervals. We will focus on the three smallest x bins where BFKL effects should become visible. Also we will only show results for the lower pseudorapidity interval, $0.5 < \eta < 1.5$, where we expect no contamination due to the fragmentation of the current jet which has not been included in the calculation. In the computation of the p_T spectra we use

$$E_e = 27.5\text{GeV}, \quad E_p = 820\text{GeV}$$

and impose the cuts which where used in the H1 measurement, i.e. we require the outgoing electron to lie in the region

$$157^\circ < \theta'_e < 173^\circ, \quad E'_e > 12\text{GeV}, \quad y > 0.05$$

in the HERA frame. Also we subtract 10% off the total cross section σ_{tot} to account for diffractive events with large rapidity gaps which have been excluded from the measurement. Finally, in the sum over the charged hadrons h in (26) we include $\pi^\pm$ and $K^\pm$, and we use the next-to-leading order fragmentation functions by Binnewies et al. [16]. In Fig. 6 we show predictions for the charged particle p_T spectrum in kinematic bin 1 of the H1 analysis with central values $x = 1.6 \times 10^{-4}$ and $Q^2 = 7$ GeV^2. We compare the results when BFKL small x resummation is included in the calculation with the case when gluon radiation is neglected. In both cases we demonstrate the effect of changing the fragmentation scale from $\mu^2 = k_j^2$ to $\mu^2 = (2k_j)^2$. We see that the BFKL prediction gives a good description of both the shape and the normalization[3] of the H1 data. On the other hand, when

[3] Even though we have normalised Φ to the DIS + jet data, there still remains some residual uncertainty in the overall normalisation associated with the choice of infrared cut-off used in the k_γ integration in (20). Our results are shown for the natural choice $k_{\gamma 0}^2 = 1$ GeV^2

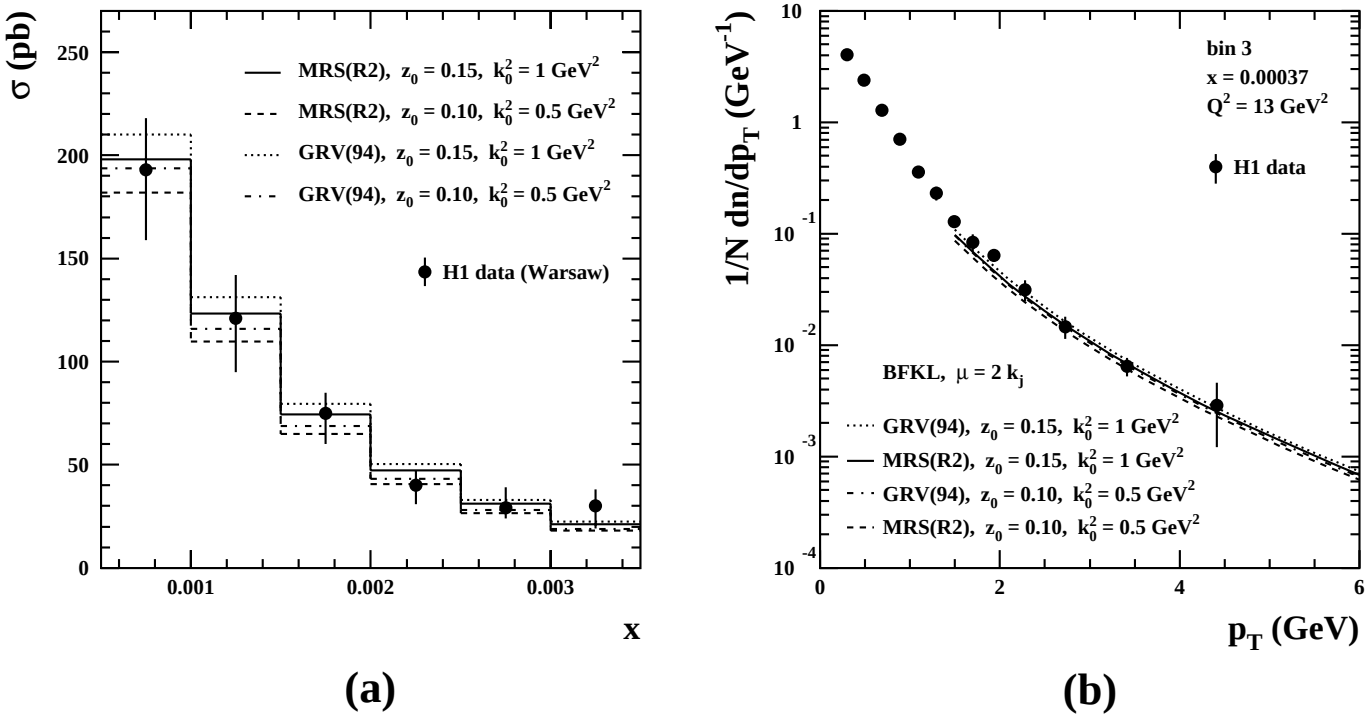

Fig. 9. The description of **a** DIS + forward jet data and **b** the charged particle transverse momentum spectrum obtained using four different choices of input. The GRV and MRS(R2) partons are taken from [17] and [15] respectively

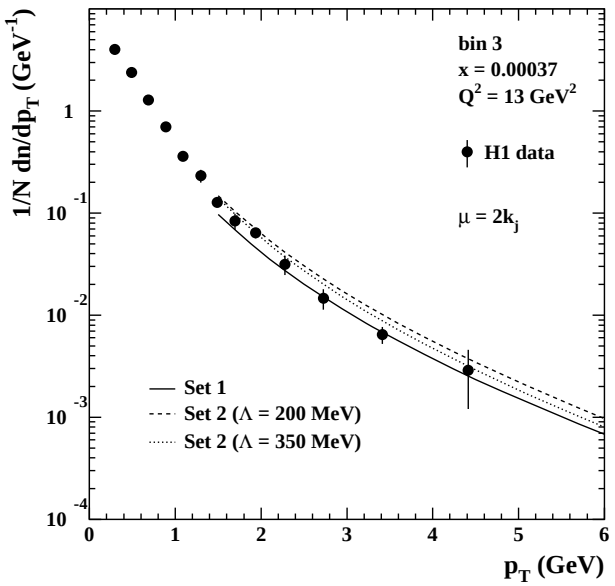

Fig. 10. The charged particle transverse momentum spectrum in kinematic bin 3 obtained using two different sets of fragmentation functions. Set 1, which was used for the previous figures, is taken from [16], and set 2 is from [18]. Set 2 is available for various choices of $\Lambda^{(4),\mathrm{NLO}}$. We show the spectrum calculated using the parametrisations corresponding to $\Lambda^{(4),\mathrm{NLO}} = 200$ MeV and 350 MeV. In all three case the fragmentation functions were evaluated at scale $\mu^2 = (2k_j)^2$. Note that set 2 describes the fragmentation of all charged hadrons whereas from set 1 we only included pions and kaons and neglected the very small contribution due to protons

the BFKL effects are neglected the predictions lie considerably below the data. Also we see, as expected, that the spectrum decreases more rapidly with p_T than when the BFKL resummation is included. For example for $p_T = 1.5$ GeV the two predictions differ by a factor 3.6, whereas for $p_T = 6$ GeV this factor is almost 10. This is a reflection of the diffusion in $\ln k_T^2$ along the BFKL ladder.

The same general behaviour is seen in Figs. 7 and 8 where we show the comparison for kinematic bins 2 and 3, with central values $x = 2.9 \times 10^{-4}$, $Q^2 = 9$ GeV^2 and $x = 3.7 \times 10^{-4}$, $Q^2 = 13$ GeV^2, respectively. We find that in all three small x bins of the H1 analysis the data support the inclusion of BFKL resummation in the calculation of the p_T spectra. Reasonable variations of the fragmentation scale do not allow for a description of the data when BFKL effects are neglected. In Fig. 9 we illustrate the sensitivity of the calculated cross sections to the choice of parton distributions and of the cut-off k_0^2 and the starting point z_0 of the BFKL evolution. For a given set of partons and a given choice of k_0^2 the value of z_0 should be chosen to give an optimal description of the DIS + jet data, Fig. 9a. This was done for MRS(R2) partons with $k_0^2 = 1\mathrm{GeV}^2$, but not for the other three choices shown so as to better display the typical variations. Even so we see that the combined description of both data sets (Figs. 9a and b) is rather stable to reasonable variations of the input choices.

We now investigate the sensitivity of the predictions to the choice of fragmentation functions. The charged particle transverse momentum spectra shown in Figs. 6–9 where calculated using the fragmentation functions given in [16] which we will refer to as set 1. Recently Binnewies [18] obtained a new set ("set 2") which for our analysis has

the advantage that the gluon fragmentation function is better constrained than in set 1. This improvement was achieved by using data for the longitudinally polarized cross section together with the now available NLO longitudinal coefficient functions. In contrast to set 1, where the authors distinguished between pions and kaons, set 2 describes the fragmentation of all charged hadrons. Also unlike set 1, where $\Lambda^{(5),\mathrm{NLO}}$ was a free parameter in the fit, for set 2 different fixed values of $\Lambda^{(4),\mathrm{NLO}}$ were used, leading to different subsets of fragmentation functions. Of these $\Lambda^{(4),\mathrm{NLO}} = 350$ MeV which corresponds to $\Lambda^{(5),\mathrm{NLO}} = 229$ MeV is closest to the value which was obtained for set 1, namely $\Lambda^{(5),\mathrm{NLO}} = 227$ MeV. In Fig. 10 we show a comparison of the charged particle spectrum in kinematic bin 3 calculated using the two sets of fragmentation functions evaluated at scale $\mu^2 = (2k_j)^2$. Displayed as a solid line is the spectrum obtained from set 1 including pions and kaons and neglecting protons. The dashed and dotted curves correspond to the spectrum for all charged hadrons calculated from set 2 for the choices $\Lambda^{(4),\mathrm{NLO}} = 200$ MeV and 350 MeV respectively. We find that using set 2 leads to an increase of the spectrum which is mainly due to the new gluon fragmentation function, see Fig. 21 in [18]. We see that the uncertainty due to fragmentation, although not negligible, is considerably less than the difference between the curves calculated using the BFKL equation and the ones in which the BFKL radiation is neglected shown in Figs. 7–9.

4 Conclusion

We studied the DIS + forward jet process including massive charm in the quark box and solving the BFKL equation numerically for running coupling. We found that BFKL dynamics describe the shape of the x distribution of the HERA data well. Next we used these data to fix the normalization of the solution of the BFKL equation with the boundary condition given by the quark box. This enabled us to give an absolute prediction for charged particle transverse momentum spectra at small x. We calculated the spectrum for large values of p_T first including BFKL small x resummation in the calculation and second neglecting gluon radiation. It turned out that the BFKL prediction agrees well with the H1 data both in shape and normalization, whereas the approximate fixed order result underestimates the data and decreases too rapidly with p_T. We may therefore conclude that the data are indicative of the existence of $\ln(1/x)$ effects and for the diffusion in $\ln k_T^2$ which accompanies BFKL evolution. Despite these encouraging results it would, however, still be useful to compare the BFKL prediction for the p_T spectrum with the result of the complete fixed order calculation[4]. Experimental data for higher values of p_T would allow an even clearer distinction between the different predictions. BFKL effects would also become more apparent in the pseudorapidity interval $-0.5 < \eta < 0.5$ which corresponds to higher values of x_j and therefore to a longer BFKL evolution starting from the quark box. Of course higher x_j also means less BFKL evolution from the proton end. This is, however, not a disadvantage, since already for the pseudorapidity interval which we considered the main contribution to the spectrum comes from the region $x_j > \bar{z}_0$. We conclude that although more experimental data especially for higher values of p_T would be useful, the existing spectra are compatible with the presence of BFKL effects at small x at HERA.

Acknowledgements. We thank Michael Kuhlen and Erwin Mirkes for their help and encouragement and Janko Binnewies for providing the code for the fragmentation functions. J.K. would like to thank the Department of Physics and Grey College of the University of Durham for their warm hospitality. S.C.L. thanks the UK Engineering and Physical Sciences Research Council for financial support. This work has been supported in part by Polish State Committee for Scientific Research Grant No. 2 P03B 089 13, by the EU under Contracts Nos. CHRX-CT92-0004 and CHRX-CT93-357, and by BMBF and DFG.

References

1. E.A. Kuraev, L.N. Lipatov, V. Fadin, Zh. Eksp. Teor. Fiz. **72**, 373 (1977) (Sov. Phys. JETP **45**, 199 (1977)); Ya. Ya. Balitzkij, L.N. Lipatov, Yad. Fiz. **28**, 1597 (1978) (Sov. J. Nucl. Phys. **28**, 822 (1978)); L.N. Lipatov, in "Perturbative QCD", edited by A.H. Mueller, (World Scientific, Singapore, 1989), p. 441; J.B. Bronzan, R.L. Sugar, Phys. Rev. **D17**, 585 (1978); T. Jaroszewicz, Acta. Phys. Polon. **B11**, 965 (1980)
2. J. Kwiecinski, A.D. Martin, A.M. Stasto, Phys. Rev. **D56**, 3991 (1997)
3. Yu. Dokshitzer, Soviet Phys. JETP **46**, 641 (1977); V.N. Gribov, L.N. Lipatov, Soviet J. Nucl. Phys. **15**, 438 (1972) 675; G. Altarelli, G. Parisi, Nucl. Phys. **B126**, 298 (1977)
4. A.H. Mueller, Nucl. Phys. B (Proc. Suppl.) **18C**, 125 (1990); J. Phys. **G17**, 1443 (1991); W.K. Tang, Phys. Lett. **B278**, 363 (1992); J. Bartels, A. De Roeck, M. Loewe, Z. Phys. **C54**, 635 (1992); A. De Roeck, Nucl. Phys. B (Proc. Suppl.) **29A**, 61 (1992); J. Kwiecinski, A.D. Martin, P.J. Sutton, Phys. Lett. **B287**, 254 (1992); Nucl. Phys. B (Proc. Suppl.) **29A**, 67 (1992)
5. J. Kwiecinski, A.D. Martin, P.J. Sutton, Phys. Rev. **D46**, 921 (1992)
6. K. Golec-Biernat, J. Kwiecinski, A.D. Martin, P.J. Sutton, Phys. Rev. **D50**, 217 (1994); Phys. Lett. **B335**, 220 (1994)
7. H1 collaboration: S. Aid et al., Phys. Lett. **B356**, 118 (1995)
8. M. Kuhlen, Phys. Lett. **B382**, 441 (1996); Contribution to the Workshop on "Future Physics at HERA", Hamburg 1996, hep-ex/9610004

[4] The approximate fixed order result, in which we neglect BFKL evolution, is based on the subprocess $\gamma^* g \to q\bar{q}g$ with the charged particle p_T spectra coming from the outgoing gluon jet. At this order this is expected to be the dominant contribution. Indeed since the fixed order calculation failed to explain the DIS + forward jet data we may anticipate that it will also be inadequate in the case of the single particle p_T distribution

9. J. Bartels, V. Del Duca, A. De Roeck, D. Graudenz, M. Wüsthoff, Phys. Lett. **B384**, 300 (1996)
10. H1 Collaboration, C. Adloff et al., contributed paper pa03-049, ICHEP '96, Warsaw, Poland, July 1996
11. M. Ciafaloni, G. Camici, contribution to the Ringberg Workshop: New Trends in HERA Physics, May 1997
12. E. Mirkes, D. Zeppenfeld, Phys. Rev. Lett. **78**, 428 (1997)
13. H1 Collaboration, C. Adloff et al., Nucl. Phys. **B485**, 3 (1997)
14. A.J. Askew et al., Phys. Rev. **D47**, 3775 (1993); **D49**, 4402 (1994)
15. A.D. Martin, R.G. Roberts, W.J. Stirling, Phys. Lett. **B387**, 419 (1996)
16. J. Binnewies, B.A. Kniehl, G. Kramer, Phys. Rev. **D52**, 4947 (1995)
17. M. Glück, E. Reya, A. Vogt, Z. Phys. **C67**, 433 (1995)
18. J. Binnewies, DESY preprint DESY-97-128, hep-ph/9707269